Phenotypic screening with 3D cell-based assays

Booij, T.H.

chapter 6

In vitro 3D phenotypic drug screen identifies celastrol as an effective *in vivo* inhibitor of polycystic kidney disease

Tijmen H. Booij[1#], Wouter N. Leonhard[2#], Kuan Yan[3], Michiel Fokkelman[1], Anna J. Plugge[2], Kimberley A.M. Veraar[2], Johannes G. Dauwerse[2], Gerard J.P. van Westen[4], Bob van de Water[1], Leo S. Price[1,3¥], Dorien J.M. Peters[2¥].

# Authors contributed equally
¥ Authors contributed equally

1 Division of Toxicology, Leiden Academic Centre for Drug Research (LACDR), Leiden University, Leiden, The Netherlands
2 Department of Human Genetics, Leiden University Medical Center (LUMC), Leiden, The Netherlands
3 OcellO B.V., Leiden, The Netherlands
4 Division of Medicinal Chemistry, Leiden Academic Centre for Drug Research (LACDR), Leiden, The Netherlands

Manuscript submitted and under revision

Abstract

Polycystic kidney disease (PKD) is a prevalent genetic disorder, characterized by the formation of kidney cysts that progressively lead to kidney failure. The currently available drug tolvaptan is not well tolerated by all patients and there remains a strong need for alternative treatments. The signaling rewiring in PKD that drives cyst formation is highly complex and not fully understood. As a consequence, the effects of drugs are sometimes difficult to predict. We previously established a high throughput microscopy phenotypic screening method for quantitative assessment of renal cyst growth. Here we applied this 3D cyst growth phenotypic assay and screened 2320 small drug-like molecules, including approved drugs. We identified 81 active molecules that inhibit cyst growth. Multi-parametric phenotypic profiling of the effects on 3D cultured cysts discriminated molecules that showed preferred pharmacological effects above genuine toxicological properties. Celastrol, a triterpenoid from *Tripterygium Wilfordii*, was identified as a potent inhibitor of cyst growth *in vitro*. In an *in vivo* iKspCre-*Pkd1*^{lox,lox} mouse model for PKD, celastrol inhibited the growth of renal cysts and maintained kidney function.

Introduction

Autosomal Dominant Polycystic kidney disease (ADPKD) affects approximately 1 in 2500[1] people that will develop renal failure as a result of progressive growth of renal cysts that interfere with normal kidney function. The disease is caused by mutations in the *PKD1*- or *PKD2* genes that encode polycystin-1 or polycystin-2, respectively.[2] These proteins are expressed in several cellular compartments and form multimeric protein complexes, that modulate several signaling pathways, which in concert control essential cellular functions such as proliferation, apoptosis, cell adhesion and differentiation. However, how mutations in the PKD genes drive the development of renal cysts is still not fully understood. In addition, we know little about how the signaling pathways involved in driving renal cyst growth, are interconnected and how they contribute to this process. As a consequence, it is also poorly understood how certain compounds that are under investigation for their therapeutic potential, exert their 'cyst-reducing' properties and why certain therapies become less effective at the more progressive stages. Currently only one drug, tolvaptan (Jinarc), is marketed for the treatment of PKD. This drug has massive diuresis as a side-effect, which may limit compliance of otherwise asymptomatic patients.[3] Because PKD patients require therapy for many decades, it is critical to improve the ba-lance between side-effects and preventing cyst growth. A possibility to achieve this goal is by combination therapy with multiple effective drugs, allowing for dose reduction, or the identification of more effective drugs with fewer side effects.

Results and discussion

To identify new drug candidates that prevent cyst growth, we developed a 3D cyst culture-based high-throughput screening platform, which can be used to screen large libraries of molecules for the identification of cyst-inhibiting compounds.[4] This 3D assay uses phenotypic profiling of cysts as a measure of compound efficacy. Phenotypic screening can enable the identification of effective molecules irrespective of their mechanism of action and without a comprehensive understanding of the pathophysiology and can be effective at identifying first-in-class treatments.[5] Here, we screened the SPECTRUM library, containing 2320 molecules including kinase inhibitors, natural molecules and FDA-approved drugs. We cultured epithelial cysts from mIMCD3 cells with short hairpin-mediated reduced *Pkd1* expression (mIMCD3 sh*Pkd1*) in 384-well plates in protein hydrogels. Following exposure to forskolin, to induce cyclic adenosine monophosphate (cAMP) production by adenylyl cyclase and subsequent cyst swelling, we co-exposed the cysts to control compounds or test compounds of the SPECTRUM library at 1μM (supplemental figure 1). After imaging and calculating cyst size using phenotypic measurement, we ranked the molecules on their potency to inhibit cyst growth as presented in figure 1A, top panel. As criterion for hit selection, molecules were selected that were at least one standard deviation below the stimulated control condition (2.5μM forskolin). As a result, 81 cyst-inhibiting hits were identified (figure 1A, bottom panel). All hits were re-screened at six concentrations in triplicate wells using RNA-guided *FokI* nuclease-mediated[6] *Pkd1*-knockout cells (mIMCD3 *Pkd1*$^{-/-}$). (Supplemental figure 2A-B), confirming the activity of 66.6% of the molecules (54 molecules with cyst growth inhibition ›50% at 1μM).

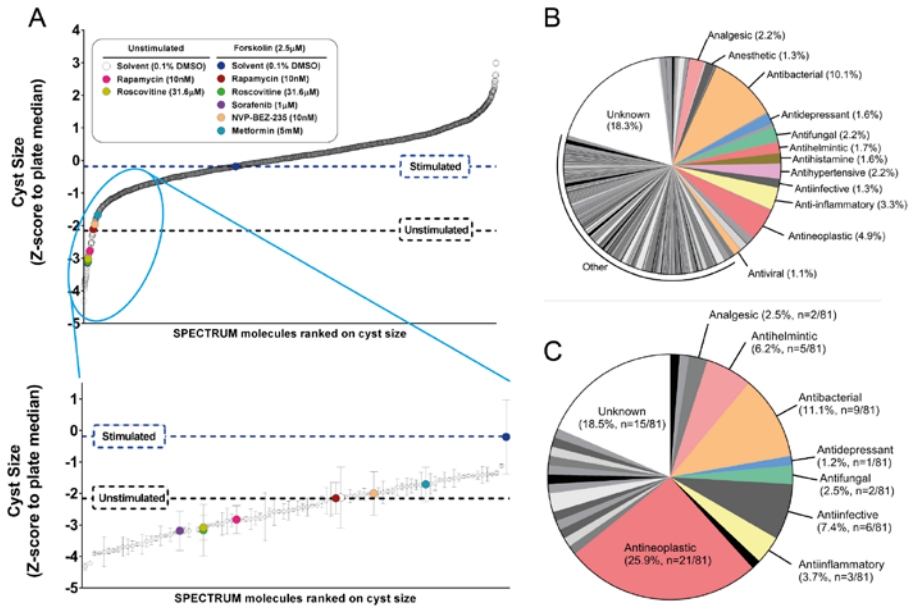

FIGURE 1 Screening a small-molecule library to identify inhibitors of cyst growth. **A)** 2320 molecules were ranked according to inhibitory effect on cyst growth on mIMCD3 sh*Pkd1* cysts (z-score normalized to plate median). Molecules inhibiting cyst growth relative to forskolin-stimulated control ("Stimulated") included positive control molecules, as indicated by colored circles in the enlarged cut-out. For control molecules, error bars represent standard deviations (SD). For all other molecules, error bars represent ½*difference between two replicate wells. **B)** Many molecules contained in the library have an antibacterial or antineoplastic mechanism of action. Since for some natural molecules the mechanism of activity is not elucidated, the bioactivity is listed as "unknown". **C)** The selected 81 cyst growth-inhibiting hits were markedly enriched in antineoplastic, anti-infective and antihelmintic molecules, compared to figure B.

To get more insight into the molecules that were active in our screen, we listed the molecules according to their bioactivities described in the manufacturer's datasheet. It is important to note that some molecules do not belong exclusively to one class and may have dual bioactivities. An evaluation of the 81 hits revealed that the largest group of selected hits were molecules known to have an antineoplastic mechanism of action (25.9% of our hits compared to 4.9% of the library) (figure 1B-C).

Since most ADPKD patients will need drug treatment for decades, antineoplastic drugs are unlikely to become therapeutic candidates. Therefore, we applied linear discriminant analysis (LDA) on measured phenotypic parameters (with correlation ‹0.85), to discriminate known toxic molecules from stimulated- and unstimulated controls.

This strategy allowed us to separate most antineoplastic molecules from molecules with a different mode of action. (supplemental figure 3A-B). For all molecules we determined the proximity in feature space to the unstimulated control group as a measure of desirable efficacy. Supplemental figure 3C presents this distance as a color scale from yellow to blue. While most anti-infective and anthelmintic retained their favorable activity (distance ‹50 at 1µM), most antineoplastic molecules remained distant from the favorable (and small) control cysts phenotype.

Based on these results, we found that celastrol (figure 2A), a triterpenoid extracted from *Tripterygium Wilfordii,*[7] and pyrvinium pamoate, an anthelmintic drug[8] and WNT inhibitor[9] (supplemental figure 4A), were very potent at inhibiting cyst growth *in vitro*. Celastrol appeared to induce phenotypes associated with toxicity only at high concentrations (≥316nM), and potently inhibited forskolin-induced cyst growth at 100nM (figure 2B-C). Pyrvinium pamoate showed no indication of toxicity even at high concentrations (supplemental figure 4B). Interestingly, we also discovered that several closely-related structural analogues of celastrol displayed a similar activity profile (supplemental figure 5A-B).

To investigate whether the inhibition shown by celastrol was dependent on cAMP induction by forskolin, we assessed whether it could inhibit cyst growth in the absence of forskolin. While more variation within wells was observed within this long-duration assay (attributable to the necessity to refresh compounds and culture media), we observed activity of celastrol at 100nM, but not 10nM, compared to solvent control (figure 2D).

To investigate whether the findings *in vitro* could be translated to a response *in vivo*, we tested both celastrol and pyrvinium pamoate in a iKspCre-*Pkd1*^{lox,lox} mouse model, where tamoxifen was used to inactivate the *Pkd1* gene at postnatal day (P) 10 and P11, to induce rapid cyst formation.[10-11] Treatment with pyrvinium pamoate from P13 appeared to be toxic at 1mg/kg/day, and lower dosages did not affect PKD progression in this model (supplemental figure 4C, 4D). We therefore did not further pursue this compound as a possible candidate for PKD treatment. By contrast, celastrol treatment inhibited PKD progression in two separate experiments. The effects of celastrol were first measured at 1mg/kg/day (7 mice) from P13-P27, and, even though changes in bodyweight were observed initially, between P13 and P18, celastrol appeared to be well tolerated. In a subsequent independent experiment, we observed similar effects of celastrol at 0.5mg/kg/day (8 mice) but not at 0.2mg/kg/day (8 mice) (supplemental figure 6A). The reduction in body weight may be related to celastrol's reported role as a leptin sensitizer,[12] and, while this finding may introduce bias (food restriction is known to ameliorate cystogenesis in patients[13]), we consider it unlikely that anti-obesity effects would explain such profound effects *in vivo* and particularly not efficacy *in vitro*. In line with the *in vitro* findings, celastrol strongly protected kidney function, while lowering cyst burden (figure 3A-C and supplemental figure 6B-E) and PKD-associated fibrosis (figure 3D-E) at 0.5 and 1.0mg/kg/day, but not at 0.2mg/kg/day.

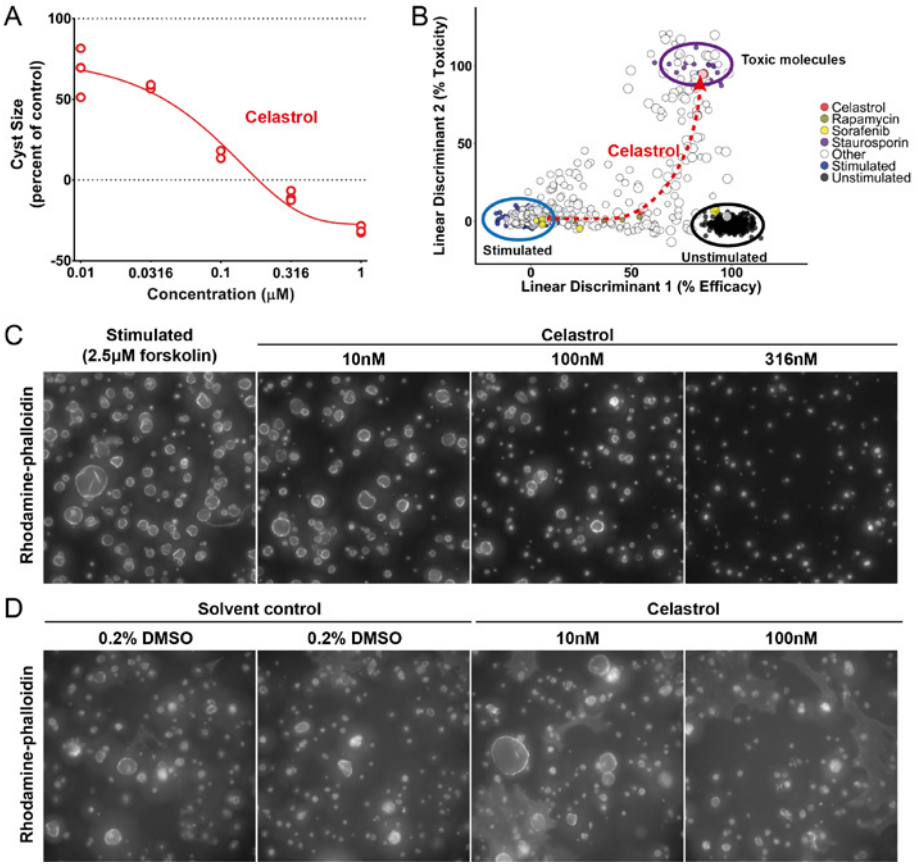

FIGURE 2 Celastrol inhibits cyst growth dose-dependently. A) Celastrol inhibits mIMCD3 *Pkd1*-/- cyst growth. At the highest concentrations (316 and 1000nM) cyst size is lower than unstimulated control, possibly corresponding to effects shown in B in linear discriminant 2. These experiments were repeated at least three times. **B)** LDA plot showing efficacy (linear discriminant 1) and toxicity (linear discriminant 2) of celastrol using multiparametric phenotypic measurements on mIMCD3 *Pkd1*-/- cysts. At the left (ringed in blue) the forskolin stimulated large cysts. At the right (ringed in black) the unstimulated small cysts. Larger dot sizes correspond to higher compound concentrations. Celastrol (red dots) is only toxic at the highest concentration. **C)** Representative images of 3D-cultured mIMCD3 *Pkd1*-/- cysts (cytoskeleton, F-actin) co-exposed with 2.5μM forskolin and celastrol at different concentrations, or vehicle control (stimulated, 2.5μM forskolin). 500x500px cut-out of images taken with the ImageXpress Micro XLS imager shown for presentation purposes. **D)** Long-term exposure with celastrol shows inhibition of spontaneous cyst growth over 13 days. 1000x1000px cutout of (cytoskeleton, F-actin) images taken with the BD Pathway 855 imager. Brightness and contrast of all images were enhanced for presentation purposes.

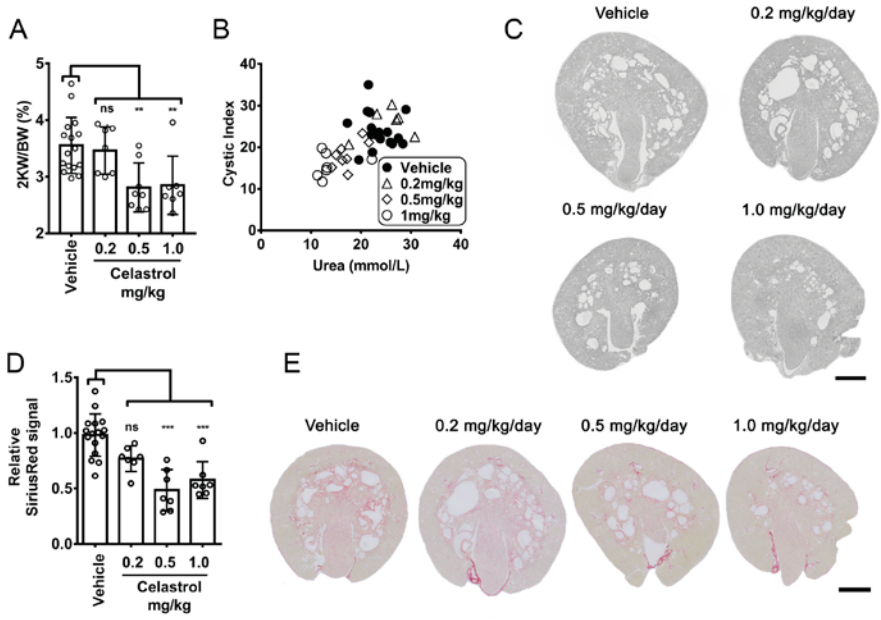

FIGURE 3 Celastrol inhibits cyst growth *in vivo* in iKspCre-*Pkd1*^{lox,lox} mice and prevents decline of kidney function. The results presented here combined two independent experiments, where celastrol was first tested at 1mg/kg/day and later at 0.2 and 0.5mg/kg/day because the vehicle controls were highly similar. **A)** Two-kidney weight as percentage of bodyweight of vehicle-treated or celastrol-treated mice at postnatal day 27. Data shown represent means ±SD and individual data points for all mice. Vehicle treated (n=16), celastrol 0.2mg/kg (n=7), 0.5mg/kg (n=8) and 1.0mg/kg (n=7). **B)** Blood urea nitrogen (BUN/Urea) given in mmol/L for vehicle- or celastrol-treated mice as a measurement of kidney function plotted against cystic index, indicating *in vivo* cyst size (disease severity) measured in P27 kidneys after vehicle or celastrol treatment. Vehicle treated (n=16), celastrol 0.2mg/kg (n=7), 0.5mg/kg (n=8) and 1.0mg/kg (n=7). **C)** Representative images of renal histology of P27 kidneys showing renal cysts are reduced after celastrol treatment for 0.5 and 1.0mg/kg treatment groups, compared to vehicle. Additional tissue sections are presented in supplemental figure 6 to illustrate experimental variation. **D)** Fibrotic index as measured by intensity of Sirius Red signal (normalized to vehicle control) for vehicle-treated (n=16), 0.2mg/kg/day celastrol-treated (n=7), 0.5mg/kg/day celastrol-treated (n=7) and 1.0mg/kg/day celastrol-treated (n=7) mice. **E)** Representative Sirius Red-stained sections of P27 kidneys of celastrol treated (0.2, 0.5 and 1.0mg/kg/day) compared to vehicle-treated. Statistical significance was assessed with ordinary one-way ANOVA with Dunnett's multiple comparisons test. *p<0.05, **p<0.01, ***p<0.001.

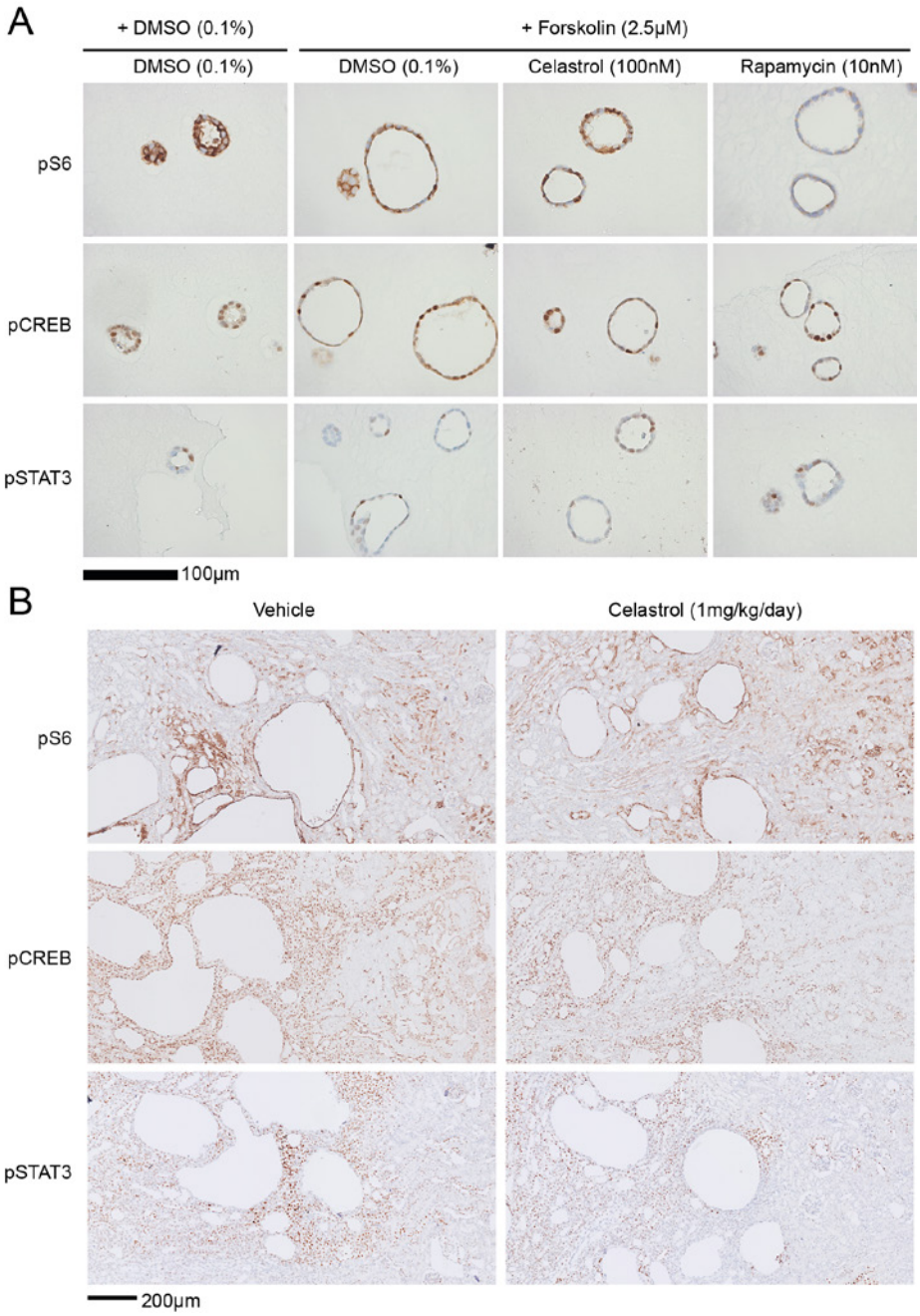

FIGURE 4 Celastrol does not affect known PKD-associated signaling. A selection of PKD-associated pathways has been analyzed. **A)** Representative images of sections of 3D-cultured mIMCD3 *Pkd1-/-* cysts, treated with solvent (DMSO), celastrol or rapamycin and stained for pS6 (mTOR activity), pCREB and pSTAT3 after fixation.
(legend continues on next page)

B) Tissue sections after staining for pS6, pCREB and pSTAT3 of vehicle-treated and celastrol-treated mice (1mg/kg/day shown). Images were made in areas were cystic and non-cystic tissue was present, to minimize bias of differential signaling associated with cystic versus non-cystic tissue (not related to celastrol treatment).

Celastrol has been investigated for other indications where it has shown promising responses, such as inflammatory disorders, cancer and obesity.[12, 14-16] However, the mechanism by which celastrol may affect cyst growth is unclear and we therefore investigated its effects on known PKD-associated signaling (pCREB, pS6, pSTAT3). Both, in 3D cyst cultures (figure 4A) and tissue sections (figure 4B), we found no effects of celastrol treatment on these targets. A variety of studies suggested a large number of signaling pathways that may be affected by celastrol including HSP90/Cdc37[17-18] and NFκB[19] (for a literature overview see supplemental table 2). We therefore consider it likely that celastrol affects cystogenesis by a multi-target mechanism. This idea was further supported by recent research by Zhou et al, where 66 celastrol-binding proteins were identified, which function in various different processes, including (redox-) metabolism and the ubiquitin proteasome pathway.[20] This multi-target mechanism may be the result of interactions of celastrol (and other triterpenoids) with thiol groups in many proteins.[20-22] Interestingly, similar Michael acceptor properties have been reported for curcumin,[23] a molecule that also delays cystogenesis in mice.[24] Because these molecules may have different affinity towards different thiol residues, it is possible that they affect other proteins and pathways as a result of concentration changes.[22] Celastrol is also known to have antioxidant activity,[25] and may therefore reduce kidney damage by induction of cytoprotective genes, as reported for curcumin,[26] which can in turn ameliorate cystogenesis.[27-29]

Conclusions

In conclusion, using phenotypic screening, we have identified celastrol as a potent inhibitor of cyst growth. We confirmed the efficacy of celastrol in a juvenile PKD model where it potently protected kidney function and lowered cyst burden. The phenotypic screening approach allowed for the identification of this molecule without knowing its mechanism of action, which is likely not specific for one target. Celastrol may prove to be an interesting treatment option for PKD, provided that it has a desirable safety- and efficacy profile.

CONCISE METHODS

3D cyst culture procedure

Cyst culture and screening was performed as described previously.[4] Briefly, cryopreserved mIMCD3 sh*Pkd1* or mIMCD3 *Pkd1*$^{-/-}$ cells were quick-thawed and grown in culture medium (DMEM/F12 Ham's, supplemented with FBS and antibiotics) for 72 hours. Cells were trypsinized and mixed with Cyst-Gel (OcellO) and plated in 384 well plates (Greiner Bio-One). After addition of culture medium, cysts were allowed to form

during 72 hours (*shPkd1*) or 96 hours (*Pkd1*$^{-/-}$) and subsequently exposed to forskolin (Calbiochem) and test compounds for 72 hours. Cysts were thereafter fixed and simultaneously stained for F-actin and nuclei for 12-24 hours at 4°C. After washing in 1x PBS (Sigma Aldrich) for 24 hours, plates were imaged using either a BD Pathway 855 microscope (BD Bioscience) or ImageXpress Micro XLS (Molecular Devices), with a 4x objective.

Image- and data analysis

Image stacks for each well were analyzed and phenotypes were quantified using Ominer software (OcellO) integrated in KNIME Analytics Platform (http://www.knime.org) (supplemental figure 1A, C). 450 phenotypic measurements were *z*-score normalized to plate median or normalized to percent of control. Linear discriminant analysis (LDA) was performed using the 83 least correlating phenotypic parameters (Pearson product-moment correlation coefficient ‹0.85). LDA was trained on unstimulated (solvent), stimulated (forskolin-treated) and known cytotoxic molecules (daunorubicin, doxorubicin, staurosporin, gambogic acid, epirubicin, at 1µM) and the trained model was applied to all data. The two resulting linear discriminants were scaled and a small absolute distance (‹50) to the unstimulated control group was considered as desirable efficacy.

Compounds

A molecule library containing 2320 compounds (SPECTRUM 2320) was obtained from MicroSource Discovery Systems. Compounds were pre-dissolved to 10mM in DMSO (Biosolve) and final DMSO content was kept constant at a well-tolerated 0.2%v/v for all *in vitro* experiments. Celastrol was derived from this library and performed equally well compared to celastrol obtained from another source (Sigma Aldrich).

Animal procedures

The local animal experimental committee of the Leiden University Medical Center (LUMC) and the Commission Biotechnology in Animals of the Dutch Ministry of Agriculture approved all animal experiments performed. Kidney specific, tamoxifen-inducible Cre-*Pkd1*lox mice (iKspCre-*Pkd1*^{lox,lox})[10, 30] received 15mg/kg Tamoxifen at postnatal day 10 and 11 to inactivate *Pkd1* to cause rapid cyst formation. Mice received i.p. injections of celastrol, pyrvinium pamoate or vehicle (5% DMSO + 10% Kolliphor EL in PBS) between P13 and P27. Mice were euthanized at P27 after blood sample collection to measure blood urea levels using Reflotron Technology. Kidneys were halved and snap frozen or embedded in paraffin. Image scans of Periodic acid-Schiff (PAS) stained kidney sections were analyzed by an investigator blinded to the treatment. The fibrotic index was calculated as done previously on the basis of Sirius Red staining.[11]

Statistical analysis

Statistical analyses were performed in Graphpad Prism 7 software using ANOVA with Dunnett's multiple comparison's test unless otherwise stated. Results were considered statistically significant for p‹0.05.

Detailed descriptions of the experimental procedures are included as supplemental methods.

Acknowledgments

T.H. Booij and W.N. Leonhard were supported by the Dutch Technology Foundation STW (Project 11823), which is part of The Netherlands Organization for Scientific Research (NWO). Gerard van Westen is supported by the Dutch technology Foundation STW (Project 14410). Michiel Fokkelman was supported by the EU-FP7 — Systems Microscopy NoE (grant no. 258068) and Anna J. Plugge by a grant from the Dutch Kidney Foundation (4OIP12).

Disclosures

L.S. Price is co-founder and CSO of OcellO B.V., a drug discovery contract research organisation located in Leiden, The Netherlands.

References

1. Willey CJ, Blais JD, Hall AK, Krasa HB, Makin AJ, Czerwiec FS: Prevalence of autosomal dominant polycystic kidney disease in the European Union. *Nephrol Dial Transplant*, 2016
2. Torres VE, Harris PC, Pirson Y: Autosomal dominant polycystic kidney disease. *Lancet* 369(9569): 1287-1301, 2007
3. Torres VE, Chapman AB, Devuyst O, Gansevoort RT, Grantham JJ, Higashihara E, Perrone RD, Krasa HB, Ouyang J, Czerwiec FS: Tolvaptan in patients with autosomal dominant polycystic kidney disease. *N Engl J Med* 367(25): 2407-2418, 2012
4. Booij TH, Bange H, Leonhard WN, Yan K, Fokkelman M, Kunnen SJ, Dauwerse J, Qin Y, van de Water B, van Westen GJP, Peters DJM, Price LS: High-throughput phenotypic screening of kinase inhibitors to identify drug targets for polycystic kidney disease. *SLAS Discov (in press)*
5. Swinney DC: Phenotypic vs. target-based drug discovery for first-in-class medicines. *Clin Pharmacol Ther* 93(4): 299-301, 2013
6. Tsai SQ, Wyvekens N, Khayter C, Foden JA, Thapar V, Reyon D, Goodwin MJ, Aryee MJ, Joung JK: Dimeric CRISPR RNA-guided FokI nucleases for highly specific genome editing. *Nat Biotechnol* 32(6): 569-576, 2014
7. Wong KF, Yuan Y, Luk JM: Tripterygium wilfordii bioactive compounds as anticancer and anti-inflammatory agents. *Clin Exp Pharmacol Physiol* 39(3): 311-320, 2012
8. Jung RC: Treatment of intestinal parasitic disease. *South Med J* 69(6): 799-804, 1976
9. Thorne CA, Hanson AJ, Schneider J, Tahinci E, Orton D, Cselenyi CS, Jernigan KK, Meyers KC, Hang BI, Waterson AG, Kim K, Melancon B, Ghidu VP, Sulikowski GA, LaFleur B, Salic A, Lee LA, Miller DM, 3rd, Lee E: Small-molecule inhibition of Wnt signaling through activation of casein kinase 1alpha. *Nat Chem Biol* 6(11): 829-836, 2010

10. Lantinga-van Leeuwen IS, Leonhard WN, van der Wal A, Breuning MH, de Heer E, Peters DJ: Kidney-specific inactivation of the Pkd1 gene induces rapid cyst formation in developing kidneys and a slow onset of disease in adult mice. *Hum Mol Genet* 16(24): 3188-3196, 2007
11. Leonhard WN, Kunnen SJ, Plugge AJ, Pasternack A, Jianu SB, Veraar K, El Bouazzaoui F, Hoogaars WM, Ten Dijke P, Breuning MH, De Heer E, Ritvos O, Peters DJ: Inhibition of Activin Signaling Slows Progression of Polycystic Kidney Disease. *J Am Soc Nephrol* 27(12): 3589-3599, 2016
12. Liu J, Lee J, Salazar Hernandez MA, Mazitschek R, Ozcan U: Treatment of obesity with celastrol. *Cell* 161(5): 999-1011, 2015
13. Warner G, Hein KZ, Nin V, Edwards M, Chini CC, Hopp K, Harris PC, Torres VE, Chini EN: Food Restriction Ameliorates the Development of Polycystic Kidney Disease. *J Am Soc Nephrol* 27(5): 1437-1447, 2016
14. Venkatesha SH, Dudics S, Astry B, Moudgil KD: Control of autoimmune inflammation by celastrol, a natural triterpenoid. *Pathog Dis* 74(6), 2016
15. Kannaiyan R, Shanmugam MK, Sethi G: Molecular targets of celastrol derived from Thunder of God Vine: potential role in the treatment of inflammatory disorders and cancer. *Cancer Lett* 303(1): 9-20, 2011
16. Liu Z, Ma L, Zhou GB: The main anticancer bullets of the Chinese medicinal herb, thunder god vine. *Molecules* 16(6): 5283-5297, 2011
17. Hieronymus H, Lamb J, Ross KN, Peng XP, Clement C, Rodina A, Nieto M, Du J, Stegmaier K, Raj SM, Maloney KN, Clardy J, Hahn WC, Chiosis G, Golub TR: Gene expression signature-based chemical genomic prediction identifies a novel class of HSP90 pathway modulators. *Cancer Cell* 10(4): 321-330, 2006
18. Dal Piaz F, Terracciano S, De Tommasi N, Braca A: Hsp90 Activity Modulation by Plant Secondary Metabolites. *Planta Med* 81(14): 1223-1239, 2015
19. Lee JH, Koo TH, Yoon H, Jung HS, Jin HZ, Lee K, Hong YS, Lee JJ: Inhibition of NF-kappa B activation through targeting I kappa B kinase by celastrol, a quinone methide triterpenoid. *Biochem Pharmacol* 72(10): 1311-1321, 2006
20. Zhou Y, Li W, Wang M, Zhang X, Zhang H, Tong X, Xiao Y: Competitive profiling of celastrol targets in human cervical cancer HeLa cells via quantitative chemical proteomics. *Mol Biosyst* 13(1): 83-91, 2016
21. Salminen A, Lehtonen M, Paimela T, Kaarniranta K: Celastrol: Molecular targets of Thunder God Vine. *Biochem Biophys Res Commun* 394(3): 439-442, 2010
22. Liby KT, Yore MM, Sporn MB: Triterpenoids and rexinoids as multifunctional agents for the prevention and treatment of cancer. *Nat Rev Cancer* 7(5): 357-369, 2007
23. Na HK, Surh YJ: Transcriptional regulation via cysteine thiol modification: a novel molecular strategy for chemoprevention and cytoprotection. *Mol Carcinog* 45(6): 368-380, 2006
24. Leonhard WN, van der Wal A, Novalic Z, Kunnen SJ, Gansevoort RT, Breuning MH, de Heer E, Peters DJ: Curcumin inhibits cystogenesis by simultaneous interference of multiple signaling pathways: in vivo evidence from a Pkd1-deletion model. *Am J Physiol Renal Physiol* 300(5): F1193-1202, 2011

25. Wang C, Shi C, Yang X, Yang M, Sun H, Wang C: Celastrol suppresses obesity process via increasing antioxidant capacity and improving lipid metabolism. *Eur J Pharmacol* 744 52-58, 2014
26. Balogun E, Hoque M, Gong P, Killeen E, Green CJ, Foresti R, Alam J, Motterlini R: Curcumin activates the haem oxygenase-1 gene via regulation of Nrf2 and the antioxidant-responsive element. *Biochem J* 371(Pt 3): 887-895, 2003
27. Happe H, Leonhard WN, van der Wal A, van de Water B, Lantinga-van Leeuwen IS, Breuning MH, de Heer E, Peters DJ: Toxic tubular injury in kidneys from Pkd1-deletion mice accelerates cystogenesis accompanied by dysregulated planar cell polarity and canonical Wnt signaling pathways. *Hum Mol Genet* 18(14): 2532-2542, 2009
28. Takakura A, Contrino L, Zhou X, Bonventre JV, Sun Y, Humphreys BD, Zhou J: Renal injury is a third hit promoting rapid development of adult polycystic kidney disease. *Hum Mol Genet* 18(14): 2523-2531, 2009
29. Malas TB, Formica C, Leonhard WN, Rao P, Granchi Z, Roos M, Peters DJ, t Hoen PA: Meta-analysis of polycystic kidney disease expression profiles defines strong involvement of injury repair processes. *Am J Physiol Renal Physiol* 312(4): F806-f817, 2017
30. Lantinga-van Leeuwen IS, Leonhard WN, van de Wal A, Breuning MH, Verbeek S, de Heer E, Peters DJ: Transgenic mice expressing tamoxifen-inducible Cre for somatic gene modification in renal epithelial cells. *Genesis* 44(5): 225-232, 2006

SUPPLEMENTAL METHODS

Cell lines and maintenance

mIMCD3 sh*Pkd1* cells, with a short-hairpin mediated knockdown of *Pkd1*, and mIMCD3 *Pkd1*$^{-/-}$, an RNA-guided FokI nuclease-mediated *Pkd1* knockout cell line (mIMRFNPKD clone 5E4), were generated previously[1] and maintained in DMEM/F12 (Ham's) culture medium (D8062, Sigma Aldrich, Zwijndrecht, Netherlands), supplemented with 10% fetal bovine serum (FBS, obtained from Gibco Fisher Scientific, Landsmeer, Netherlands), glutamax and penicillin/streptomycin in 175cm^2 culture flasks (Corning). Before reaching maximal confluence, the monolayers were washed with 1x PBS (Sigma Aldrich, Zwijndrecht, Netherlands) and subsequently trypsinized with 1x Trypsin (Gibco Fisher Scientific, Landsmeer, Netherlands) and subsequently passaged to a new culture flask. Cell passage numbers were kept below 20 for all experiments. For cryopreservation, trypsinized cells were pelleted by centrifugation at 1500rpm for 5 minutes and the cell pellet was subsequently mixed with freezing medium consisting of 90% FBS and 10% DMSO (Biosolve B.V., Valkenswaard, Netherlands) at a concentration of 9*10^6 cells per mL and subsequently slow-frozen to -150°C.

3D cyst culture procedure

mIMCD3 sh*Pkd1* or mIMCD3 *Pkd1*$^{-/-}$ cells were quick-thawed and cultured in 175cm^2 culture flasks 72 hours prior to initiation of the 3D cultures. 3D cyst cultures were prepared as described previously.[1] Briefly, cells were trypsinized and subsequently pelleted by centrifugation. The cell pellet was mixed with Cyst-Gel (OcellO B.V. Leiden, Netherlands) at a cell density of 3*10^6 cells per mL. Using a CyBi Selma 96 automated liquid handler (Analytik Jena AG, Jena, Germany), cell-gel mix was transferred to Greiner µClear 384 well plates (Greiner Bio-One B.V. Alphen aan den Rijn, Netherlands), 14.5µL per well, at a final cell density of 2175 cells per well. After 30 minutes of gel polymerization at 37°C, 33.5µL culture medium was added and cells were grown for 72 hours (mIMCD3 sh*Pkd1* cells) or 96 hours (mIMCD3 *Pkd1*$^{-/-}$) at 37°C (5% CO_2) to initiate lumen formation, prior to compound exposures. Subsequently, cells were co-exposed with 2.5µM forskolin (*Coleus forskohlii,* Calbiochem, Millipore B.V., Amsterdam, Netherlands), to enhance cyst swelling due to the activation of adenylyl cyclase to produce cAMP, and compounds, using either the CyBi Selma 96 (for smaller scale experiments), or, to screen compound libraries, a BioMek FXP (Beckman Coulter B.V., Woerden, Netherlands) equipped with a 96-tip pipetting head. After 72 hours of compound exposures, plates were fixed with 4% formaldehyde (Sigma Aldrich, Zwijndrecht, Netherlands), permeabilized with Triton X-100 (Sigma Aldrich, Zwijndrecht, Netherlands) and stained with rhodamine-phalloidin (Sigma Aldrich, Zwijndrecht, Netherlands) and Hoechst 33258 (Sigma Aldrich, Zwijndrecht, Netherlands) for cytoskeleton and nuclei, respectively, for 12 to 24 hours at 4°C. After fixation and staining, plates were washed with 1x PBS for 24 hours and sealed with an aluminium plate seal (Greiner Bio-One B.V. Alphen aan den Rijn, Netherlands) and subsequently stored at 4°C prior to imaging (the screening procedure is schematically presented in supplemental figure 1).

Long-term 3D cyst culture procedure without forskolin

3D cyst cultures of mIMCD3 *Pkd1*$^{-/-}$ cells were prepared as described in the previous section. 33.5µL of culture medium was added to the prepared cultures, and cells were allowed to form cysts for 96 hours prior to compound exposures. 3D cultured cysts were exposed to 100nM celastrol or solvent (0.1% DMSO) in a final volume of 60µL. After 96 hours, 30µL medium/compound mix was aspirated using a CyBi Selma 96, and 18µL fresh medium and 2x 6µL fresh compound was added. After 96 hours, the cysts were fixed with 4% formaldehyde and further processed as described above.

Compounds

A (SPECTRUM) compound library with 2320 molecules was obtained from MicroSource (MicroSource Discovery Systems, Inc., Gaylordsville, Connecticut, USA). Compounds were pre-dissolved to 10mM in DMSO. Analytical grade DMSO was obtained from Biosolve B.V. (Valkenswaard, Netherlands). Rapamycin, sorafenib tosylate, roscovitine and NVP-BEZ-235 were obtained from SelleckChem (Munich, Germany). Metformin HCl was obtained from Sigma Aldrich (Zwijndrecht, Netherlands). Celastrol was obtained from two different sources (MicroSource Discovery Systems, Inc., Gaylordsville, Connecticut, USA for the primary screen and Sigma Aldrich, Zwijndrecht, Netherlands for further validation experiments and animal experiments). Both sources performed equally well in terms of cyst growth inhibition *in vitro* (not shown).

Fluorescence microscopy

384 well plates of the SPECTRUM screen were imaged using an automated (wide-field) BD Pathway 855 imager (BD Biosciences, Breda, Netherlands) with a 4x Olympus objective, coupled to a Twister II robotic arm, as described previously[2]. Subsequent experiments were imaged using an ImageXpress Micro XLS wide field high-content analysis system (Molecular Devices, Sunnyvale, CA, USA) with a 4x objective. *xy*-images were made in the *z*-direction for each well, requiring approximately 25 images for each well. Images captured with the BD pathway microscope captured approximately 70% of each well, whereas images made with the ImageXpress imager could capture the entire well.

Image- and data analysis

Image stacks for each well were analysed and phenotypes were quantified as described previously,[1] using Ominer software integrated in KNIME Analytics Platform (KNIME version 3.1.2, Konstanz, Germany, http://www.knime.org/). 450 phenotypic measurements were *z*-score normalized to plate median, or normalized to percent of control (100% corresponding with forskolin-stimulated control median and 0% with unstimulated/vehicle control median). For heatmap plots of efficacy, data was scaled between 0% inhibition of cyst growth (forskolin-stimulated control median) and 100% inhibition (unstimulated control median) for presentation purposes. Linear discriminant analysis (LDA) for the validation screen was performed using an R script (https://www.r-project.org/) integrated in KNIME. In order to remove most highly correlating phenotypic parameters prior to training the LDA, we applied a correlation filter (Pearson product-moment correlation coefficient ‹0.85 or ›-0.85) to all 450

phenotypic parameters to filter out the 367 most highly correlating parameters. The LDA model was subsequently trained based on unstimulated control (solvent, 0.2% DMSO), stimulated control (2.5μM forskolin) and known cytotoxic molecules in the library (epirubicin, doxorubicin, daunorubicin, staurosporin and gambogic acid, at 1μM concentration) and thereafter applied to all data, yielding two linear discriminants, linear discriminant 1 (LD1) and linear discriminant 2 (LD2). Linear discriminants were thereafter scaled from 0 to 100% (labelled % efficacy and % toxicity for LD1 and LD2, respectively, for presentation purposes). The phenotypic descriptors and their coefficients that were included in the linear discriminants are presented in supplemental table 1 (top 10 ranked features only). While LD1 strongly separated unstimulated (0.2% DMSO) controls from stimulated controls (2.5μM forskolin), LD2 exclusively discriminated (un)stimulated conditions from known toxic molecules. The absolute distance to the unstimulated control group for all data points was calculated based on these scaled linear discriminants and presented as a heatmap plot using the ggplot2 package (http://ggplot2.org) for Rstudio 0.99.878 (https://www.rstudio.com/products/rstudio2) with R3.2.3 (https://www.r-project.org/). S-curve plots were made using the ggplot2 package. 3D scatterplots presented in the supplemental figures were generated with the Scatterplot3D package (https://CRAN.R-project.org/package=scatterplot3d)[3] in R3.2.3. Density plots were generated with ggplot2 for R and other charts were generated with Graphpad Prism 7 (Graphpad Software, La Jolla, California, USA).

Animal procedures

The local animal experimental committee of the Leiden University Medical Center (LUMC) and the Commission Biotechnology in Animals of the Dutch Ministry of Agriculture approved all animal experiments performed.

To assess the efficacy of celastrol *in vivo* we used kidney–specific, tamoxifen–inducible Cre-*Pkd1*lox mice (iKspCre-*Pkd1*^{lox,lox}).[4-5] To inactivate the *Pkd1* gene, mice received 15mg/kg Tamoxifen (in 1% ethanol in sunflower oil, dissolved by sonication) by oral gavage at post-natal day (P)10 and P11. From P13-P27, mice received intraperitoneal injections (i.p.) of either celastrol, pyrvinium pamoate (PP) or vehicle (5% DMSO + 10% Kolliphor EL in phosphate buffered saline). After the last injection at P27, blood samples were collected from the tail vein to assess the Blood Urea levels using Reflotron Technology and then the mice were euthanized by cervical dislocation. Kidneys were cut in halves and either snap frozen in liquid nitrogen or fixed in buffered 4% formaldehyde solution for embedding in paraffin. Total image scans of Periodic acid–Schiff (PAS) stained kidney sections (4μm) were processed semi-automatically using Photoshop software by an investigator who was blinded to the treatment, as done previously.[6] Briefly, a specifically designed colour palette was used for all images to remove all pixels from the lumens/cysts, leaving only the pixels of the actual tissue. From these numbers, the percentage of 'cystic' pixels versus total number of pixels was calculated and defined as the cystic index.

Fibrotic Index

The fibrotic index was calculated as done previously on the basis of Sirius Red staining.[6] Briefly, tissue sections were stained after deparaffinization with 0.2% phosphomolybdic acid for 1 minute and 0.1% Sirius Red (in picric acid) for 90 minutes. This was followed by saturated picric acid and subsequently by ethanol/xylol washstep. Adobe Photoshop (Adobe Systems, Inc. San Jose, California, USA) was used for the quantification of Sirius Red.

Immunohistochemistry on 3D cyst cultures and tissue sections.

Samples were subjected by O/N Formaldehyde fixation (in buffered 4% Formaldehyde solution) and embedded in paraffin. For immunohistochemical analysis, 4mM sections were deparaffinised and subjected to heat-mediated antigen retrieval (10mM/1mMTris/EDTA) [pH 9.0] for anti-p (Tyr705) STAT3 [no. 9145; Cell Signaling Technology], and 10 mM citrate buffer [pH 6.0] for antiphospho-CREB [Ser133], and anti-phospho-ribosomal protein S6 (Ser240/244) from Cell Signaling Technology (no's. 9198, and 2215 respectively).

Sections were blocked with 0.1% H2O2 for 20 min for endogenous peroxidase activity and preincubated for 1 h with 5% normal goat serum in 1% BSA in PBS. Next, the sections were incubated O/N with anti-pSTAT3 (1:75), anti-p-rpS6 (1:100) or anti-pCREB (1:800). After incubation with rabbit Envision horseradish peroxidase (no. K4011;Dako) or rabbit anti-goat horseradish peroxidase (1:100; no. P0449;Dako), immune reactions were revealed using diaminobenzidine as a chromogen, counterstained with hematoxylin, dehydrated, and mounted.

Statistical Analysis

Statistical analyses were performed in Graphpad Prism 7 software, using one-way ANOVA coupled to Dunnett's multiple comparison's adjustment unless otherwise stated. Results were considered statistically significant with $p<0.05$, and this is further annotated in figure legends.

References belonging to supplemental methods

1. Booij TH, Bange H, Leonhard WN, Yan K, Fokkelman M, Kunnen SJ, Dauwerse J, Qin Y, van de Water B, van Westen GJP, Peters DJM, Price LS: High-throughput phenotypic screening of kinase inhibitors to identify drug targets for polycystic kidney disease. *SLAS Discov (in press)*
2. Booij TH, Klop MJ, Yan K, Szantai-Kis C, Szokol B, Orfi L, van de Water B, Keri G, Price LS: Development of a 3D Tissue Culture-Based High-Content Screening Platform That Uses Phenotypic Profiling to Discriminate Selective Inhibitors of Receptor Tyrosine Kinases. *J Biomol Screen* 21(9): 912-922, 2016
3. Ligges U, Mächler M: Scatterplot3D - an R Package for Visualizing Multivariate Data. *J Stat Soft* 8(11): 1-20, 2003

4. Lantinga-van Leeuwen IS, Leonhard WN, van de Wal A, Breuning MH, Verbeek S, de Heer E, Peters DJ: Transgenic mice expressing tamoxifen-inducible Cre for somatic gene modification in renal epithelial cells. *Genesis* 44(5): 225-232, 2006
5. Lantinga-van Leeuwen IS, Leonhard WN, van der Wal A, Breuning MH, de Heer E, Peters DJ: Kidney-specific inactivation of the Pkd1 gene induces rapid cyst formation in developing kidneys and a slow onset of disease in adult mice. *Hum Mol Genet* 16(24): 3188-3196, 2007
6. Leonhard WN, Kunnen SJ, Plugge AJ, Pasternack A, Jianu SB, Veraar K, El Bouazzaoui F, Hoogaars WM, Ten Dijke P, Breuning MH, De Heer E, Ritvos O, Peters DJ: Inhibition of Activin Signaling Slows Progression of Polycystic Kidney Disease. *J Am Soc Nephrol* 27(12): 3589-3599, 2016

SUPPLEMENTAL MATERIALS

SUPPLEMENTAL TABLE 1 Parameter contributions to LDA

LDA feature coefficients (top 10 negatively ranked)

LD1		LD2	
Feature Name	**Interpretation**	**Feature Name**	**Interpretation**
nc.Mean(zernike_order_1_1).meas		nc.Mean(std_child_to_par_center_dist).corr.meas	(related to position of nuclei)
actin.Mean(lumen_avg_width).struct.meas	(lumen size)	actin.Mean(lumen_avg_width).struct.meas	(lumen size)
actin.Sum(area).meas	(cyst wall size)	nc.Mean(avg_child_to_par_boundary_dist).corr.meas	(related to position of nuclei)
actin.Mean(zernike_order_2_2).meas		actin.SD(child_count).corr.meas	
actin.Mean(axis_Ratio_Minor_Major).meas	(cyst wall shape related)	actin.Mean(zernike_order_2_2).meas	
nc.Sum(area).meas	(nuclear size)	org.SD(axis_Ratio_Minor_Major).meas	(cyst shape related)
actin.Mean(eccentricity).meas	(cyst wall shape related)	nc.SD(number_of_branches).meas	
org.Count*(area).meas	(number of cysts)	actin.Mean(eccentricity).meas	(cyst wall shape related)
nc.Mean(child_parent_size_ratio).corr.meas	(nuclear size relative to cyst)	nc.Sum(area).meas	(nuclear size)
nc.SD(maximum_intensity).meas		nc.Mean(solidity).meas	(nuclear roundness)
LDA feature coefficients (top 10 positively ranked)			
nc.Mean(maximum_intensity).meas	(staining intensity of nuclei)	nc.Mean(hu_order_1).meas	
org.Mean(number_of_single_junction_points).meas		actin.SD(eccentricity).meas	(cyst wall shape related)
nc.Mean(avg_child_to_par_boundary_dist).corr.meas	(related to position of nuclei)	org.Mean(axis_Ratio_Minor_Major).meas	(cyst shape related)
nc.Mean(number_of_end_points).meas		nc.SD(maximum_intensity).meas	(nuclear intensity)
nc.Mean(hu_order_1).meas		nc.SD(zernike_order_8_2).meas	
actin.Mean(std_intensity).meas	(actin intensity related)	actin.SD(child_parent_size_ratio).corr.meas	(related to thickness of cyst wall)
nc.SD(zernike_order_8_2).meas		actin.Mean(std_intensity).meas	(actin intensity related)
actin.SD(eccentricity).meas	(cyst wall shape related)	org.Mean(feret).meas	
nc.SD(ratio_Area_BoundingBox_Area).meas	(nuclear shape related)	actin.Sum(area).meas	(cyst wall size)
org.Mean(feret).meas	(cyst shape related)	nc.Mean(zernike_order_1_1).meas	

SUPPLEMENTAL TABLE 2 Pathways affected by celastrol

Pathways/Targets	Context	Pubmed ID	DOI
HIF-1, erythropoietin, VEGF, mTOR, P70S6K, eIF4E, Erk	Hepatocellular carcinoma	28242743	10.1124/mol.116.107706
NFκB	Acute hepatic dysfunction	28189063	10.1016/j.etap.2017.02.002
NOX2-derived ROS-dependent PP5-JNK signaling pathway	ROS induced neurodegenerative disorders	28129433	10.1111/jnc.13966
Lipid synthesis, Sirt1		28123944	10.1016/j.molmet.2016.11.002
Nrf2, Erk1/2, Nox2, Angiotensin II type 1 receptor		28119074	10.1016/j.ejphar.2017.01.027
IKKß		27931154	10.1080/13880209.2016.1241809
Cdc37, Annexin A2, eEF1A		27819370	10.1039/c6mb00691d
HSP90/Cdc37		27398312	10.1002/2211-5463.12081
NF-kappa B, MAPK, JAK/STAT and RANKL/OPG pathways	Autoimmune inflammation	27405485	10.1093/femspd/ftw059
IRAKs to block TLR4-mediated NFκB activation	Autoimmune inflammation	27181127	10.1016/S2095-4964(16)60257-1
miR-21/ERK	Cardiac fibrosis and cardiac dysfunction	27160852	10.1159/000445554
TLR4/MyD88/NFκB	Diabetic liver injury	27057550	10.1155/2016/2641248
AMPK/PGC1α/Sirt3	Diabetic myopathy and oxidative stress	27049825	10.3892/ijmm.2016.2549
miR-21/mTOR/p27	Gastric cancer	26500453	10.1186/s12935-015-0256-3
Autophagy		26473737	10.1371/journal.pone.0140745
HSP90		17010675	10.1016/j.ccr.2006.09.005
Calpain		18726991	10.1002/jcp.21565
hERG channel	Cancer	25866772	10.1155/2015/308475
Apoptosis mediated through mitochondrial dysfunction, Akt, PI3K, 4E-BP1, mTOR. Celastrol also inhibited the Akt/GSK3beta and Akt/NFκB survival pathways	Triple-negative breast cancer	25818165	10.1016/j.yexmp.2015.03.031
CYP1A2, CYP2C19, CYP2D6, CYP2E1 and CYP3A4		25811791	10.3109/00498254.2014.1003113
HIF-1 induction through ROS/Akt/p70S6K		25383959	10.1371/journal.pone.0112470
HSP90		24954307	10.1016/j.bbagen.2014.06.008
HIF-1α pathway by inhibition of mTOR/p70S6K/eIF4E and ERK1/2		24859482	10.3892/or.2014.3211
Cannabinoid receptory type 2	Neuropathic pain	25101848	10.3390/ijms150813637
NFκB	Inflammation	PMC4453024	10.5483/BMBRep.2015.48.3.147
Inhibit proteasome and upregulate *hsp30* and *hsp70* gene expression		20188206	10.1016/j.cbpa.2010.02.015
miR-21, PI3K/Akt, NFκB		24434352	doi: 10.1159/000357683
JNK, PTEN-Akt/mTOR pathway	Cadmium-induced neuronal cell death	24111524	10.1111/jnc.12474
Snail/E-cadherin	TGF-beta induced EMT	23850675	10.1016/j.bbrc.2013.06.113
Hsp70, Akt1, p70/S6K, ERK1/2	C2C12 myotube atrophy	23810294	10.1016/j.abb.2013.06.006
LOX-1	Atherosclerosis	23799016	10.1371/journal.pone.0065477
UDP-glucuronosyl transferase (UGT) 1A6 and 2B7		22669039	10.3390/molecules17066832
p-JNK, p-c-Jun, NFκB	Cerebral ischemia	22575561	10.1016/j.brainres.2012.04.054
Estrogen receptor α (ERα)	Breast cancer	20934245	10.1016/j.canlet.2010.09.006
Platelet activation (P-selectin and glycoprotein IIb/IIIa activation)		19661812	10.1097/FJC.0b013e3181b21472
VEGFR		18343027	10.1016/j.canlet.2008.01.043

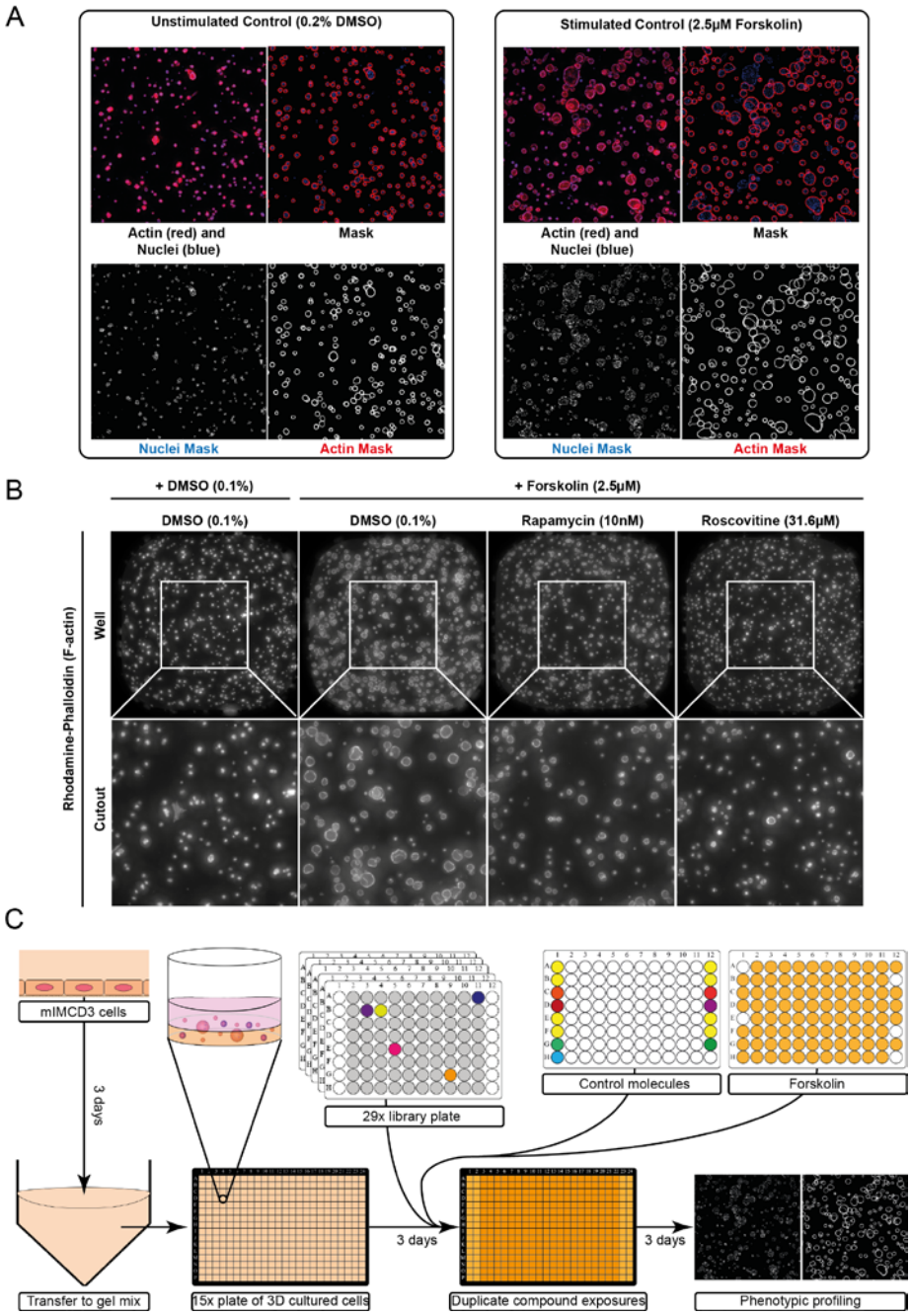

› SUPPLEMENTAL FIGURE 1 Screening molecule libraries using 3D cultured cysts. **A)** mIMCD3 *Pkd1-/-* cysts cultured for 96 hours in Cyst-Gel and exposed to solvent (unstimulated) or forskolin (stimulated). Image stacks of rhodamine-phalloidin and Hoechst 33258-stained cysts (top left images) processed by Ominer software to

(legend continues on next page)

generate- and quantify binary masks. **B)** mIMCD3 *Pkd1-/-* cells were cultured for 96 hours in Cyst-Gel and exposed to solvent (DMSO) or control compounds (rapamycin, roscovitine) in the presence of forskolin. Cytoskeleton (F-actin) shown. Upper panel shows projected image stacks of entire well images with an ImageXpress micro XLS imager. Lower panel represents 500x500px cut-out of the centre of the well. Contrast and brightness enhanced for presentation purposes. **C)** Schematic representation of screening pipeline as described under supplemental methods. mIMCD3 sh*Pkd1* cells were mixed with Cyst-Gel and allowed to develop into small cysts during 72 hours, prior to exposure to the small molecule library. Control molecules were added to the outer plate columns, and forskolin was added to all wells, except for a few wells that served as 'unstimulated' controls (16 per plate). Staurosporin was added to the lower right corner of each plate to serve as positive control for cytotoxicity. After 72-hours incubation, cultures were stained, imaged and quantified as described in the supplemental methods section.

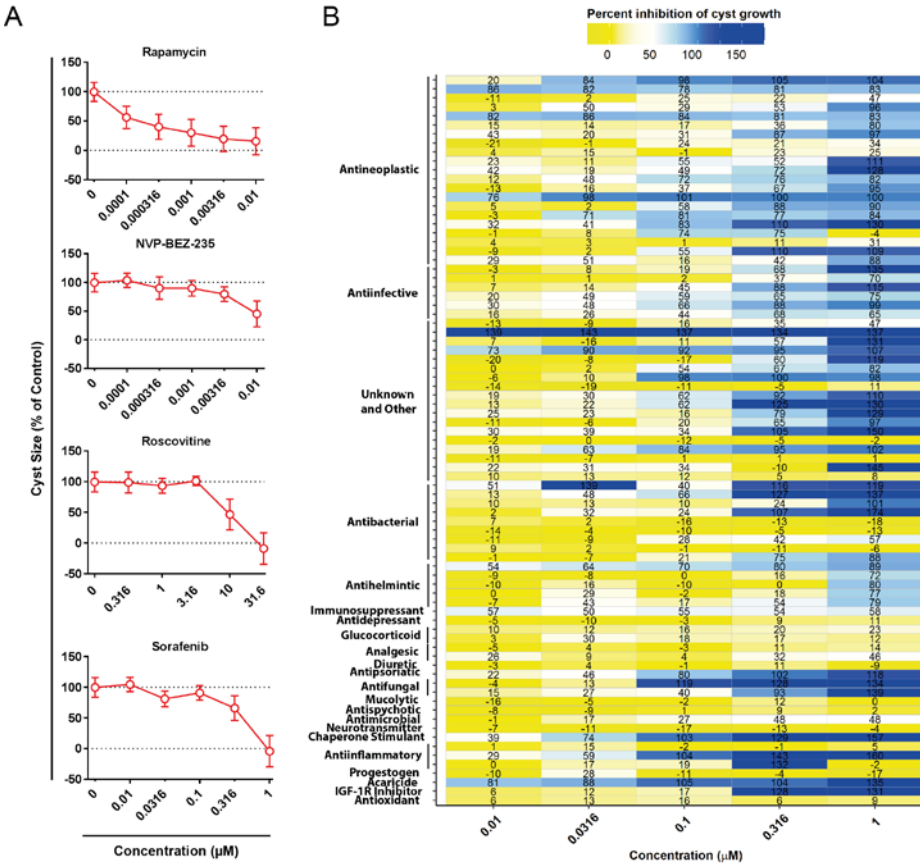

SUPPLEMENTAL FIGURE 2 Screen validation on mIMCD3 *Pkd1-/-* cysts. A) Concentration-response curves of positive control molecules in the validation screen. Cyst size was scaled to %-cyst growth: 100% represents forskolin-stimulated control (large cysts), 0% represents unstimulated control (small cysts). Means ± SD shown from triplicate wells. **B)** 81 cyst-growth inhibition molecules rescreened at 5 concentrations. Described bioactivity of the manufacturer's datasheet displayed on y-axis. Potency of molecules represented by percent- inhibition of forskolin-induced cyst growth, as represented by the colour scale and the numbers displayed (means of triplicate wells). 52/81 molecules showed activity >50% inhibition at 1mM concentration.

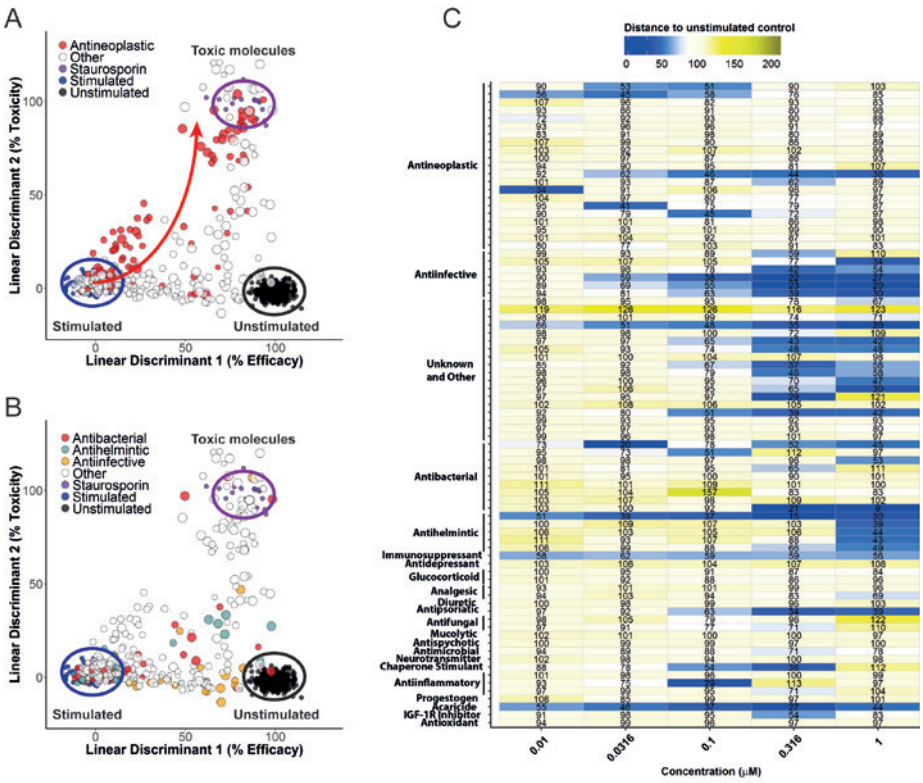

SUPPLEMENTAL FIGURE 3 Linear discriminant analysis discriminates antineoplastic molecules. **A-B)** LDA was trained as described in supplemental methods (using phenotypic parameters with linear correlation ‹0.85) and could discriminate antineoplastic molecules (A, red circles) from the unstimulated- and stimulated controls, indicated by black and blue circles, respectively, while retaining activity of others such as antibacterial (B, red circles), antihelmintic (B, light blue) or antiinfective molecules (B, yellow). Point size corresponds with concentration and points shown represent means of triplicate wells (except for "Stimulated", "Unstimulated" and "Staurosporin": individual datapoints shown). **C)** Measurement of desirable efficacy -similar to supplemental figure 2B, but presenting absolute distance to unstimulated control calculated from supplemental figure 3B, presented as colour scale and numeric values. Blue colours indicate efficacy.

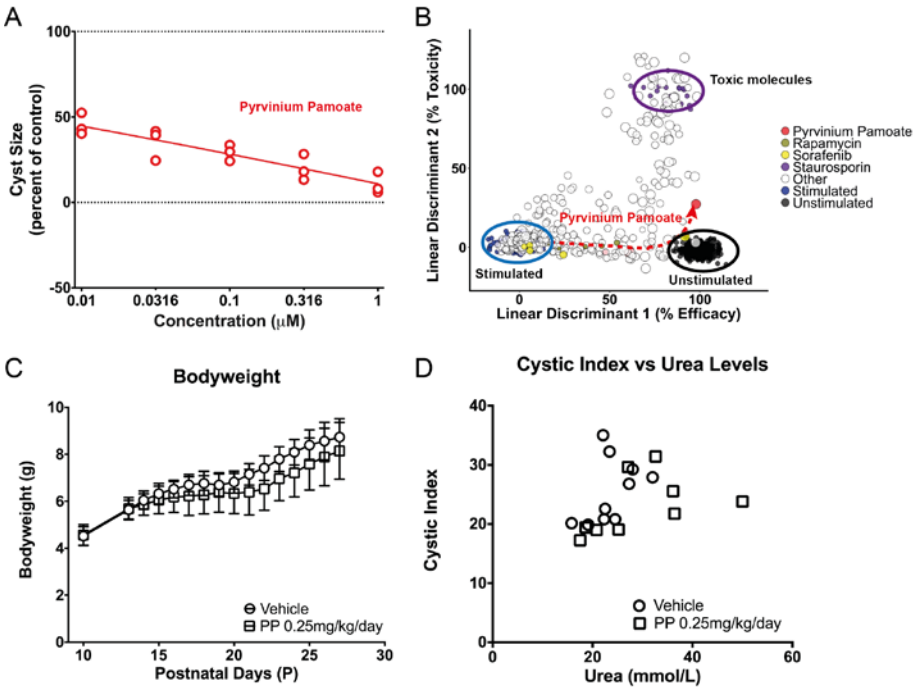

SUPPLEMENTAL FIGURE 4 Pyrvinium Pamoate (PP) shows potent efficacy *in vitro*, but not *in vivo*. **A)** PP inhibits forskolin-induced cyst growth of mIMCD3 *Pkd1*$^{-/-}$ cysts (100%, forskolin-stimulated; 0%, unstimulated). Individual wells shown as red circles. **B)** LDA plot indicates potent desirable efficacy of PP, and indicates no toxic effects. **C)** In total 17 mice received with PP treatment at postnatal day 13. Ten of those started at 1mg/kg/day of which three mice died within 4-6 days after the start of the treatment. As PP was poorly tolerated at 1mg/kg/day, we reduced the dosage for the 7 remaining mice to 0.25mg/kg/day. In order to obtain sufficient group size, 7 mice were included later during the experiment and were only treated with 0.25mg/kg/day. PP did not affect bodyweight at 0.25mg/kg/day. (vehicle n=11, PP n=14, mean ± SD shown). **C)** At 0.25mg/kg/day, PP did not lower cystic index or urea levels (vehicle n=10 and PP n=9 shown).

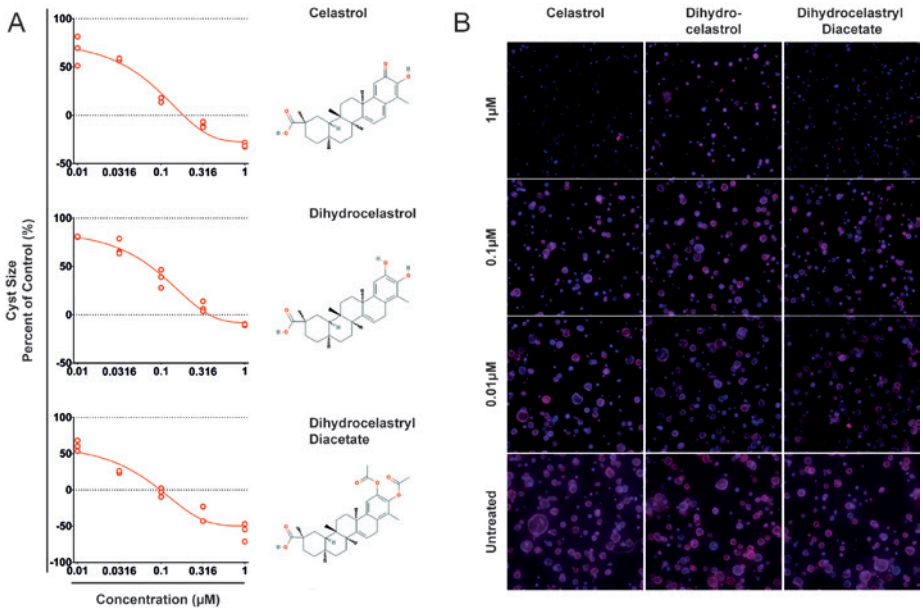

SUPPLEMENTAL FIGURE 5 Structural analogues of celastrol also potently inhibit forskolin-indued cyst growth *in vitro* in mIMCD3 *Pkd1-/-* cysts. **A)** Dihydrocelastrol (middle panel) and dihydrocelastryl diacetate (bottom panel) were included in the molecule library and inhibited forskolin-induced cyst growth similarly to celastrol (top panel). Structural formulae shown on the right were obtained from PubChem. **B)** Representative images of celastrol-treated, dihydrocelastrol-treated or dihydrocelastryl diacetate-treated mIMCD3 *Pkd1-/-* cysts. Images shown are collapsed-stack images of nuclei (Hoechst 33258, blue) and F-actin (rhodamine-phalloidin, red) combined. Images show a 500x500px cut-out from the center of the well. Images were taken with the ImageXpress micro XLS imager. Untreated control condition represents forskolin stimulated controls (corresponding with 100% cyst size in figure A).

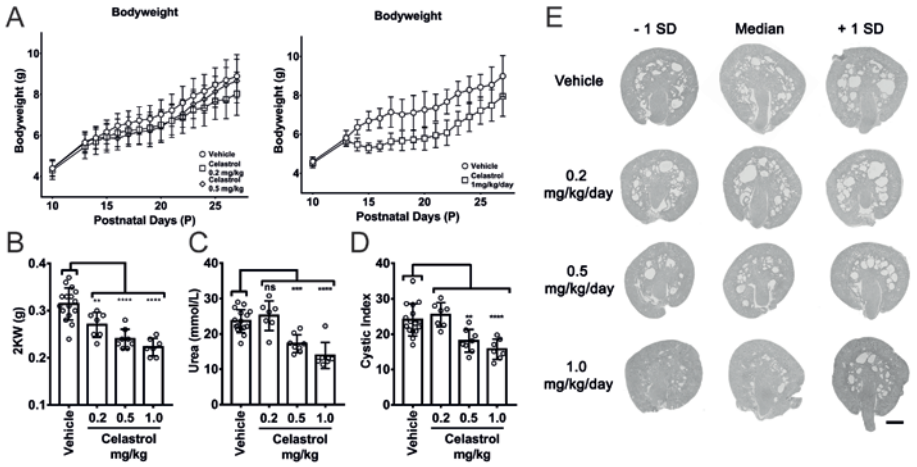

SUPPLEMENTAL FIGURE 6 Celastrol potently inhibits cystogenesis in an *in vivo* model of PKD. **A)** Bodyweight is affected by 1mg/kg/day and 0.5mg/kg/day between P13 and P18. B-D) Treatment with 0.5 and 1mg/kg/day celastrol lowers two-kidney weight **(B)**, urea levels **(C)** and cystic index **(D)** as compared to vehicle control. For these charts, we pooled the experimental data of two independent experiments (0.2 and 0.5mg/kg/day versus 1mg/kg/day celastrol), because the vehicle controls were highly similar. Mean ± SD as well as individual mice shown. *p<0.05, **p<0.01, ***p<0.001, ****p<0.0001 with ordinary one-way ANOVA with Dunnett's multiple comparison's test. **E)** Histology reveals that celastrol potently inhibited cyst growth at 0.5 and 1mg/kg/day. Images displaying cystic index close to median ±1SD were selected and presented here.